http://dx.doi.org/10.5012/bkcs.2013.34.4.1199

Binder-free Sn/Graphene Nanocomposites Prepared by Electrophoretic Deposition for Anode Materials in Lithium Ion Batteries

Eun Gyoung Bae, Yun-Hwa Hwang, and Myoungho Pyo*

*Department of Printed Electronics Engineering in WCU Program, Sunchon National University, Sunchon, Chonnam 540-742, Korea. *E-mail: mho@sunchon.ac.kr*
Received December 12, 2012, Accepted January 28, 2013

Nanocomposites consisting of Sn nanoparticles and graphene oxide (GO) were electrophoretically deposited onto Cu current collectors that was used for anodes in Li ion batteries (LIBs). In order to optimize the electrochemical performance of nanocomposites as an anode material by controlling the oxygen functionality, the GO was subjected to O_3 treatment prior to electrophoretic deposition (EPD). During thermal reduction of the GO in the nanocomposites, the Sn nanoparticles were reduced in size, along with the formation of SnO and/or SnO_2 at a small fraction, relying on the oxygen functionalities of the GO. The variation in the duration of time for the O_3 irradiation resulted in a small change in total oxygen content, but in a significantly different fraction of each functional group in the GO, which influenced the Sn nanoparticle size and the amount of SnO (and/or SnO_2). As a result, the EPD films prepared with the GO that possessed the least amount of carboxylic groups (made by treating GO in an O_3 environment for 3 h) showed the best performance, when compared with the nanocomposites composed of untreated GO or GO that was O_3-treated for a duration of less than 3 h.

Key Words : Graphene oxide, Ozonization, Electrophoretic deposition, Tin, Li ion batteries

Introduction

Metallic Tin (Sn) that possesses a relatively high theoretical capacity (994 $mAh{\cdot}g^{-1}$)[1] is considered to be a promising alternative to graphite anodes (372 $mAh{\cdot}g^{-1}$) for the development of next-generation lithium ion batteries (LIBs) with high-energy density.[2] Tin, however, shows a serious decay in reversible capacity during repeated charge-discharge (C-D) cycles, mainly due to the irreversible large volume increase accompanied by lithium incorporation. To circumvent this problem, metal oxides (*e.g.*, SnO_2) and intermetallic compounds (*e.g.*, SnSb) have been proposed. Although amorphous Li_2O produced during the first few cycles in SnO_2 or stepwise volume increase in SnSb can accommodate the volume strain to some extent, the dimensional expansion of as much as 350% eventually leads to electrical disconnection arising from the crumbling and pulverization of the Sn domains.[3]

Sn was also composited with carbonaceous materials, in which the latter can buffer the volume strain and help the maintenance of the structural integrity of Sn domains.[4] Sn/carbon,[4b] Sn/graphene,[4d,4e] and their hybrids[4c] with regulated nanostructures have been investigated. Most of these combinations have proven to be effective, revealing that the preparation of composites with carbonaceous materials, represented by graphene, is a promising strategy in developing a new anode for LIBs with high-energy density.

EPD is an economical and convenient method used to deposit film directly on a conducting substrate.[5] The EPD processing technique has been extensively utilized in diverse fields, such as solar energy conversion devices,[6] field emission devices,[7] and phosphor deposition for displays.[8] EPD also is utilized for the preparation of binder-free cathodes[9] and anodes.[10] Binder-free graphite anodes by EPD were investigated and utilized as an effective anode in a molten salt electrolyte.[10a,10b] Recently, Ui *et al.* reported the fabrication of a binder-free SnO_2 anode by EPD.[10c] They addressed the phenomenon whereby SnO_2 nanoparticles co-deposited with acetylene black show relatively high capacity retention (504 $mAh{\cdot}g^{-1}$ after 50 C-D cycles at 0.1 C).

Herein, we describe the preparation of EPD films, consisting of Sn nanoparticles and GO, and their use as anode materials in Li ion batteries. To the best of our knowledge, an electrophoretically deposited nanocomposite of GO and Sn has not been studied as an anode for LIBs.

Figure 1 schematizes the concept of this work. the deposition rate and film quality were controlled by adjusting the concentration of Mg^{2+} in a deposition bath. The subsequent thermal reduction of GO was accompanied by a breakage of Sn nanoparticles (*ca.* 150 nm) into smaller pieces (*ca.* 20 nm), depending on the relative compositions of the functional groups of oxygen in the GO, which were dependent of

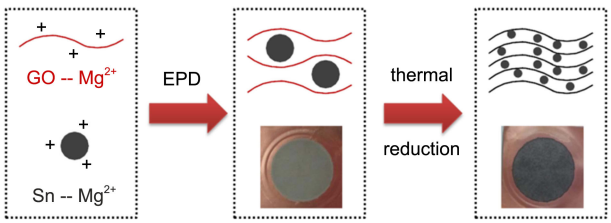

Figure 1. Schematic diagram depicting the concept of this study. Homogeneous films were produced on Cu by EPD, due to surface-adsprbed Mg^{2+}. Subsequent thermal treatment converted GO to reduced graphene and large Sn (*ca.* 150 nm) to small Sn nanoparticles (*ca.* 20 nm).

the ozonization time of the GO. The best electrochemical performance was attained for the film containing the GO with the fewest carboxylic groups.

Experimental

Ozonization of GO. Single layer graphene oxide (GO), which has a thickness of 0.7-1.2 nm, was purchased from Cheap Tubes Inc., USA and used as received. In order to examine the effect of ozonization on the oxygen functionalities of the GO and, thus, the EPD process, the GO was subjected to ozonization (AHTECH Ltd.) for 1, 3, and 5 h. Hereafter, as-such prepared GO will be designated by GO-1, GO-3, and GO-5, respectively (untreated GO by GO-0).

Preparation of Sn/GO Films by EPD. Go (3 mg) and Sn nanoparticles (3 mg, ≤ 150 nm, Aldrich) were dispersed in 15 mL isopropyl alcohol (≥ 99.5%, Aldrich) by sonication for 15 min. $Mg(NO_3)_2{\cdot}6H_2O$ (99%, High purity chemicals) was subsequently added to the dispersion to facilitate the deposition on a negative electrode during application of an electric field. Without Mg^{2+}, Sn/GO composite films were formed on a positive electrode, but the film surface was quite irregular, due to weak adhesion of GO to the substrate.[7a,11] The relative concentration of the Mg^{2+} to the GO also affected both the film quality and the deposition rate. When the weight ratio of Mg^{2+} to GO was smaller than 0.1, the film seemed loosely packed and the deposition rate was so slow that the precipitation of Sn nanoparticles was unavoidable. For densely packed nanocomposite films that could be obtained within a relatively short period of time (30 min), we found that the minimal ratio of Mg^{2+} to GO was 0.1. EPD was performed using a home-made cell. Cu was used for both positive and negative electrodes (≥ 99.8%, Nippon Foil Mfg. Co.). A DC voltage (EC 570, E-C Apparatus Corp.) of 300 V was applied between the two electrodes, separated by 23 mm. The films deposited for 30 min (Sn/GO-0, Sn/GO-1, Sn/GO-3, and Sn/GO-5 for the nanocomposite films deposited using GO-0, GO-1, GO-3, and GO-5, respectively) were washed with copious amounts of anhydrous ethanol and dried under ambient conditions. The nanocomposites were thermally treated in a tube furnace to reduce the GO (Sn/rGO-0, Sn/rGO-1, Sn/rGO-3, and Sn/rGO-5 for the reduced Sn/GO-0, Sn/GO-1, Sn/GO-3, and Sn/GO-5, respectively). The temperature was increased to 500 °C at a heating rate of 10 °C·min^{-1} and was maintained for 2 h under Ar.

Characterization. The evolution of the characteristic diffraction peaks of the GO after the ozonization and oxidation of Sn nanoparticles during thermal treatment were examined using a powder X-ray diffractometer (XRD, Rigaku ULTIMA 4). The distribution of the Sn nanoparticles on the GO was investigated using a Hitachi S3500 field emission scanning electron microscope (FESEM). X-ray photoelectron spectroscopy (XPS) studies were carried out using a Thermo Fisher (K-Alpha) electron spectrometer with an Al K_α X-ray source (excitation energy = 1486.6 eV). The energy scale was adjusted with respect to the carbon peak (C_{1s}) spectrum at 284.5 eV. Thermal gravimetric analysis (TGA, Q50, TA Instruments) was performed at 10 °C·min^{-1} to quantitatively determine the oxygen functionalities.

Cell Fabrication and Electrochemical Performance. The EPD films on the Cu substrate were punched (1.6 cm in diameter) and then welded to a stainless steel case to fit in coin cells of type CR 2032. Coin cells of a Li/electrolyte/nanocomposite configuration, in which the separator was sandwiched between 2 electrodes, were assembled in an Ar-filled glove box (O_2, H_2O < 1 ppm). The separator was a Celgard 2400 microporous polypropylene membrane wetted in the electrolyte. The $LiPF_6$ was dissolved in a mixture of ethylene carbonate (EC) and dimethylcarbonate (DMC) (50:50 vol%) to a concentration of 1.0 M. A charge-discharge (C-D) test was performed using an automatic WBCS 3000 battery cycler (WonATech) in a potential range of 0.001-2.5 V *vs.* Li/Li$^+$. All assembled cells were stored at least 1 h at room temperature before testing.

Results and Discussion

Ozonization of GO. As-received single layer GO (GO-0) was first characterized by XRD. Figure 2(a) shows a weak (001) diffraction peak at 2θ of 11.68°, which corresponds to an inter-layer spacing (*d*-spacing) of 7.56 Å, indicating a lack of long-range order. No strong diffraction at 2θ of 26.5°, ascribed to graphitic domains (JCPDS no. 41-1487), was observed. The TGA of GO-0 (inset in Figure 2) also indicated an amount of oxygen functionalities of 31.7 wt %, which agreed well with the values reported previously for GO.[12] GO-0 was subjected to ozonization to confirm the change in oxygen functionalities and the effect on electrochemical performances of an anode in a composite. It is obvious that a peak position of the (001) diffraction shifted to a lower diffraction angle, with the increase in the O_3 irradiation time. GO-1 and GO-3 showed gradual increases of *d*-spacing (8.51 and 8.66 Å, respectively). This implies that the O_3-treatment of GO can affect the oxygen functionalities either by the increase in total oxygen content or by the change in the relative compositions of various types of oxygen groups. Interestingly, further ozonization again reduced the *d*-spacing to 8.13 Å, as shown in Figure 2(d). This seems to suggest

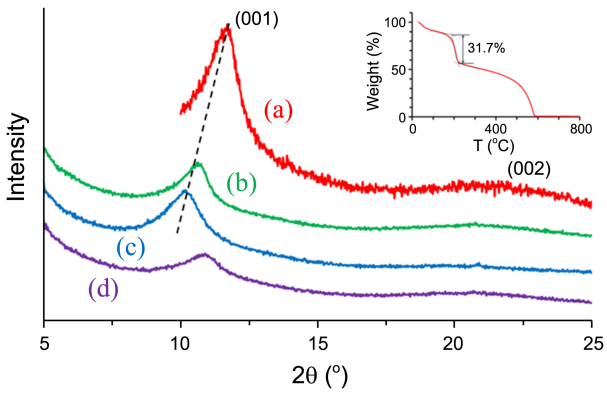

Figure 2. XRD patterns of (a) GO, (b) GO-1, (c) GO-3, and (d) GO-5. Inset shows a TGA curve of GO-0 in air.

Table 1. Binding energy (BE) and atomic % (at %) of different chemical states of carbon, obtained from high-resolution XPS spectra

Chemical state	O-C=O		C=O		C-O-C		C-OH		C=C or C-C	
	BE	at %	BE	at %	BE	at %	BE	at %	BE	at %
GO-0	289.41	7.1	288.14	10.8	287.32	42.2	286.03	11.0	285.31	28.9
GO-1	289.41	8.2	288.18	12.1	287.31	40.9	286.08	13.6	285.31	25.2
GO-3	289.41	6.8	288.14	11.1	287.32	38.8	286.03	19.1	285.31	24.2
GO-5	290.81	10.6	288.96	26.3	287.35	29.4	286.27	10.6	285.45	23.1

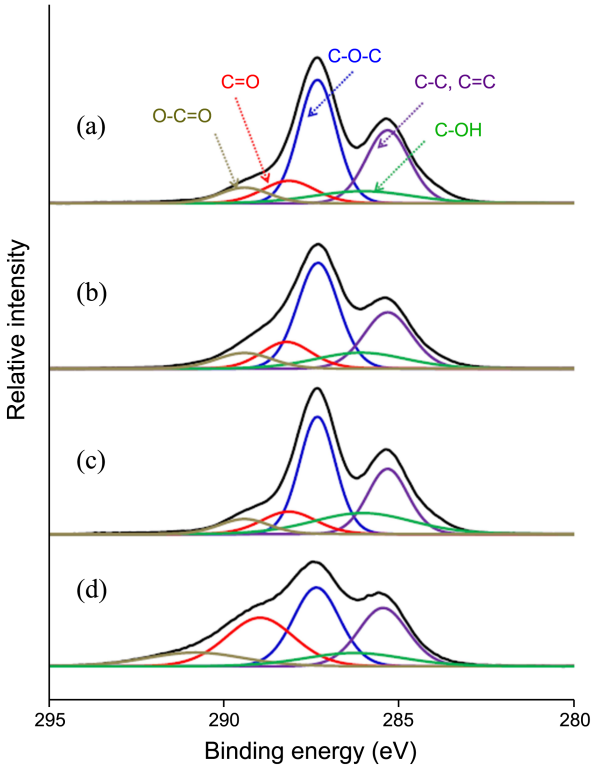

Figure 3. High-resolution XPS spectra of (a) GO, (b) GO-1, (c) GO-3, and (d) GO-5.

that the variation in the *d*-spacing is more dependent on the types of functional groups rather than on the total amount of oxygen groups, because lengthening the ozonization time continuously increased the amount of oxygen relative to carbon (see below).

To further examine the effect of ozonization on GO, XPS studies were carried out. The relative atomic % of oxygen to carbon (O/C) was determined from the XPS survey scan spectra. As expected, O/C increased with O_3-irradiation. The O/C of 0.56 for GO-0 was increased to 0.60, 0.61, and 0.62 for GO-1, GO-3, and GO-5, respectively. To confirm whether the increase in oxygen wt% means a simultaneous increase in the fraction of all the types of functional groups, the high-resolution XPS spectra of the C1s were examined. The XPS spectra, shown in Figure 3, indicated the presence of five different chemical states of carbon in GO. The main oxygen functional groups in GO are known to be epoxide, hydroxyl, carbonyl, and carboxyl moieties.[13] Figure 3 also validates the presence of these functional groups at different binding energies, along with C1s single- and/or double-bonded to carbon.[14] With O_3-irradiation, however, the relative compositions of each functional group were significantly changed, as represented by the continuous decrease in the epoxide peak heights from GO-0 to GO-5 and by the sudden shift in a carboxylic peak position from GO-3 to GO-5 (This may be due to a shake-up satellite at high biding energy tail.).

The deconvolution results of the spectra are summarized in Table 1. Note that the content for C-C and C=C was continuously decreased with O_3-treatment, corresponding to the change in O/C from the survey scan. For GO-1 and GO-3, the atomic % of O-C=O, C=O, and C-O-C varied within an experimental uncertainty of quantification by XPS. C-OH, however, noticeably increased with ozonization. GO-5, on the other hand, showed a rather abrupt deviation from this trend. The significant increase in the atomic % of O-C=O and C=O was offset by a sharp decrease in the atomic % of C-O-C and C-OH. Since the carbonyl and carboxylic groups have been known to be present on the edge of graphene sheets, the sudden increase in these functional groups in GO-5 appears to imply that ozonization for 5 h caused a breakage of carbon networks, producing more peripheral sites. It is noteworthy that the atomic % of C-OH was the greatest in GO-3, which is correlated to the distribution of Sn nanoparticles on graphene layers after thermal reduction.

The similar behaviors were also confirmed from FTIR studies. Figure 4 indicates that all the samples show characteristic peaks of GO at 1059 (epoxy C-O), 1223 (carboxyl O-H), 1375 (carboxyl C-O), 1610 (aromatic C=C), and 1730 cm^{-1} (carbonyl and carboxyl C=O).[15,16] It was evident that the intensity of C=O relative to C=C increased from Figure

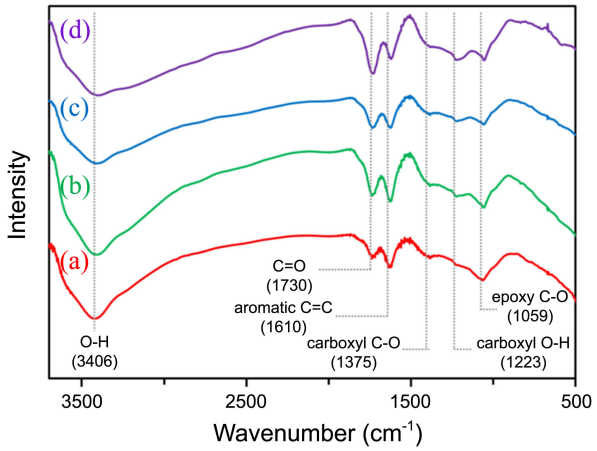

Figure 4. FTIR spectra of (a) GO, (b) GO-1, (c) GO-3, and (d) GO-5.

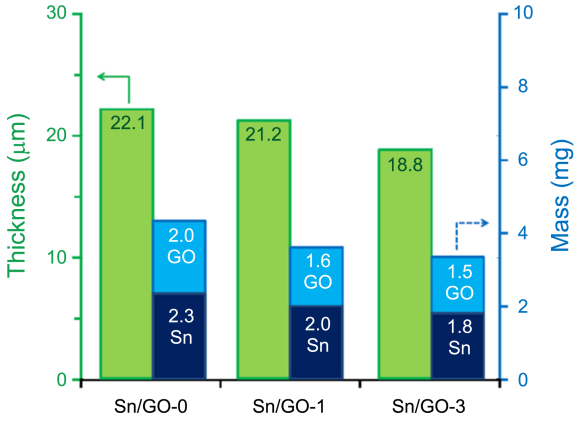

Figure 5. Film thickness and mass changes by EPD for 30 min. The amount of Sn was calculated from thermogravimetric analysis under air, assuming that all Sn was converted to SnO_2 and GO was completely decomposed.

4(a) to 4(d), corresponding to XPS interpretations.

Preparation of Nanocomposites by EPD and Subsequent Thermal Reduction. EPD was performed in an isopropanol medium containing Sn nanoparticles (*ca.* 150 nm) and GO. Since GO-5 showed the substantial deviation from general trends (abnormal decrease of d-spacing and change in oxygen functionalities), we used GO-0, GO-1, and GO-3 for EPD. Figure 5 shows thickness and mass changes with an ozonization time. It is interesting that, as more functionalized GO was used, the amount of composites deposited on Cu was decreased. It seems because GO with more functional groups interacts woth more Sn nanoparticles through Mg^{2+} ions, which results in a reduction of electrophoretic mobility.[5]

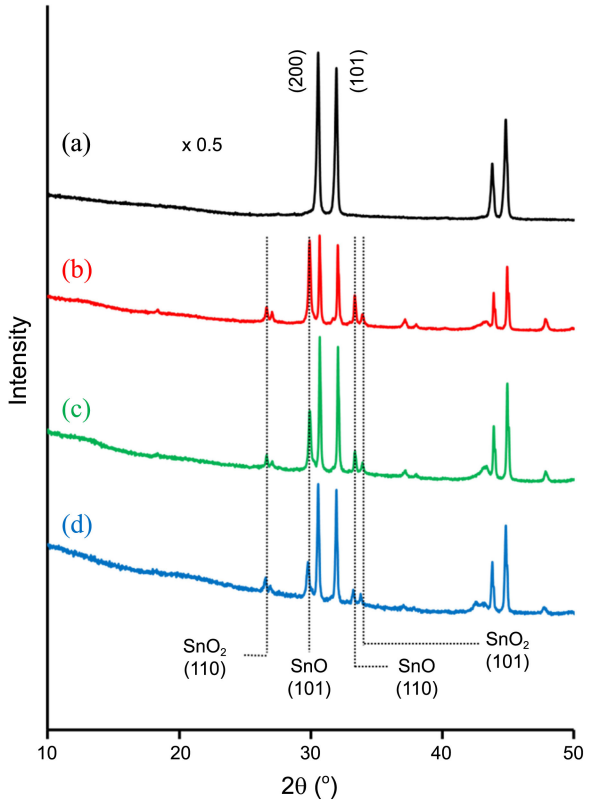

Figure 6. XRD patterns of (a) Sn/GO-0, (b) Sn/rGO-0, (c) Sn/rGO-1, and (d) Sn/rGO-3.

The nanocomposite films were thermally treated at 500 °C in Ar to reduce the GO. Figure 6(a) shows the XRD pattern of Sn/GO-0 (*i.e.*, before thermal treatment), which matches well with that of β-Sn (JCPDS no. 86-2265, body-centered tetragonal). Following the treatment of Sn/GO-0 at 500 °C, a substantial fraction of the Sn was transformed to SnO (JCPDS no. 06-0395, *ca.* 20 nm in diameter) along with a trace amount of SnO_2 (JCPDS no. 41-1445, *ca.* 20 nm in diameter). The amount of SnO and SnO_2 was reduced gradually from Sn/rGO-0 to Sn/rGO-1 and to Sn/rGO-3. Note that the relative peak height of SnO(101) to Sn(200) is decreased from Figure 6(b) to Figure 6(c) and to Figure 6(d) (The comparison of reference intensity ratio values using integrated peak intensities gave the same results.). Since the only oxygen source was GO, the reduction in the amount of SnO was interesting. We believe that the formation of a SnO phase was related to the oxygen functional groups of GO.

Since Sn nanoparticles should melt during the thermal reduction at 500 °C, the change in Sn morphologies was also examined. Figure 7(a) shows an FESEM image of Sn/GO-0. It is evident that Sn nanoparticles with diameters of *ca.* 150 nm were well-composited with GO, but some nanoparticles were agglomerated. On the contrary, Figure 7(b) indicates that the thermal treatment substantially changed both the particle size and distribution of Sn nanoparticles. The formation of Sn nanoparticles with a small size (*ca.* 20 nm), sacrificing pristine Sn (*ca.* 150 nm), is distinct. Figures 7(c) and 7(d) show that the formation of small Sn nanoparticles became more conspicuous for the composites consisting of more ozonized GO. In Sn/rGO-3, the pristine Sn was hardly seen and nearly all Sn was *ca.* 20 nm in size.

The reduction in SnO content and in Sn size after thermal reduction of the composite with more ozonized GO was likely due to the different oxygen functionalities of GO. XPS studies revealed that the ozonization caused a substantial increase in the hydroxyl moiety in the GO, while the rests

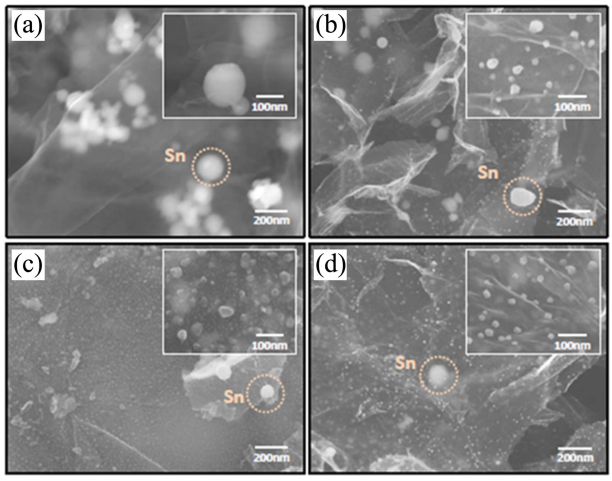

Figure 7. FESEM images of (a) Sn/GO-0, (b) Sn/rGO-0, (c) Sn/rGO-1, and (d) Sn/rGO-3.

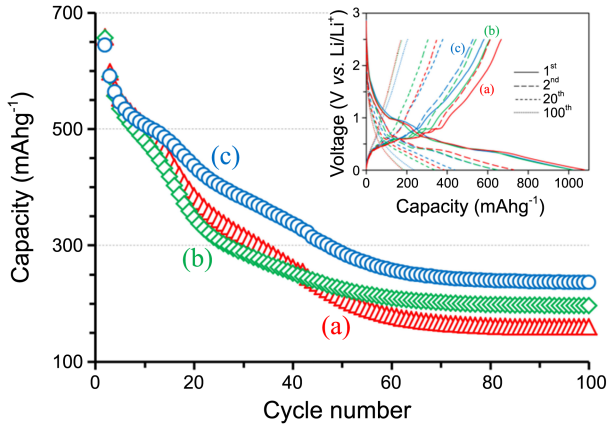

Figure 8. Discharge capacity retention of (a) Sn/rGO-0, (b) Sn/rGO-1, and (c) Sn/rGO-3. Inset shows C-D profiles of the 1st, 2nd, 20th, and 100th cycles. Current density = 100 mA·g^{-1}.

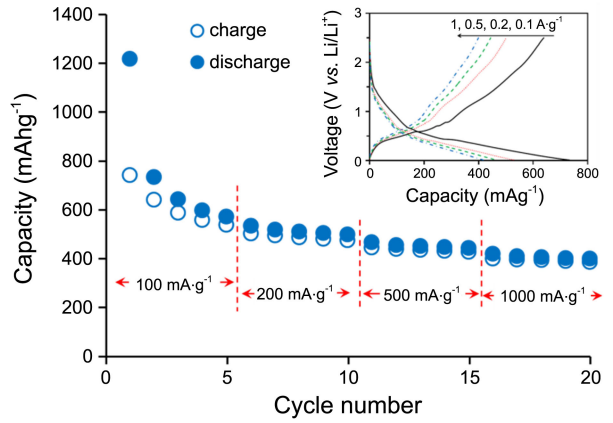

Figure 9. Rate capability of Sn/rGO-3. Inset shows C-D profiles of the 2nd cycle after changing current density.

(carboxyl, carbonyl, epoxide) remained invariant within the experimental error (see Figure 3 and Table 1). Since the thermal decomposition of oxygen functional groups and Sn melting occur in a similar temperature range , XPS analysis is likely to suggest that the hydroxyl groups attract more strongly with melted Sn and, thus, more hydroxyl groups creates smaller Sn particles. The decrease in SnO content in Sn/rGO-1 and Sn/rGO-3 appears to be related to the reduction in oxygen content from the carboxyl, carbonyl, and epoxide groups.

Electrochemical Performance of the Nanocomposites. Expecting the best capacity retention and rate capability for Sn/rSG-3, resulting from well-dispersed small Sn nanoparticles on graphene layers,[17] charge-discharge (C-D) tests were performed for Sn/rSG-0, Sn/rSG-1, and Sn/rSG-3. Figure 8 shows the discharge (Li alloying) capacity retention during 100 C-D cycles. While the initial reversible capacities are similar, the enhanced dimensional stability of Sn nanoparticles with diameters of ca. 20 nm made Sn/rSG-3 show the least capacity fading. The capacities of 236, 196, and 159 mAh·g^{-1} for Sn/rSG-0, Sn/rSG-1, and Sn/rSG-3, respectively, after 100 cycles were related to the size of Sn nanoparticles. It is worth to mentioning that the capacity value and fading were comparable to, or better than, the results reported previously.[4,18] Moreover, considering the capacity based on the composite (*i.e.*, absence of the binder and conducting additives as in previous reports), Sn/rSG-3 would be a promising material in the development of advanced anodes.

The rate capability was also examined for Sn/rSG-3. Figure 9 exhibits an excellent rate capability. The discharge capacities of 733 mAh·g^{-1} at 100 mA·g^{-1} were reduced to 532, 466, and 417 mAh·g^{-1} at 200, 500 and 1000 mA·g^{-1}, respectively. The capacity beyond 400 mAh·g^{-1} at 1000 mA·g^{-1} is exceptional for alloying/dealloying Sn anodes, when considering the previous reports.[4c,18] For example, Xu *et al.* addressed about 300 mAh·g^{-1} for porous carbon/Sn composites anodes.[18] Comparable results (417 mAh·g^{-1} at 1000 mA·g^{-1}) have been claimed by Liang *et al.*,[4c] in which carbon-coated Sn was embedded in graphene layers. The excellence of the rate capability in Sn/rSG-3 is also ascribed to the evenly distributed nanometric Sn, which was formed during thermal reduction of ozonized GO.

Conclusion

Composite films composed of Sn and GO were prepared on Cu by EPD. Ozonized GO was used for EPD because ozonization affected the relative fractions of various functional groups. GO ozonized for 3 h possessed the highest content of hydroxyl groups, which contributed to the formation of nanometric Sn during the thermal reduction of the GO. Due to evenly distributed nanometric Sn, the Sn/rGO-3 showed the best capacity retention and rate capability.

Acknowledgments. This research was supported by the WCU program through the Korea Science and Engineering Foundation funded by the Ministry of Education, Science and Technology (R31-10022).

References

1. (a) Winter, M.; Besenhard, J. O. *Electrochim. Acta* **1999**, *45*, 31.
2. (a) Prabakar, S. J. R.; Han, S. C.; Singh, S. P.; Lee, D. K.; Sohn, K.-S.; Pyo, M. *J. Power Sources* **2012**, *209*, 57. (b) Han, S. C.; Singh, S. P.; Hwang, Y.-H.; Bae, E. G.; Park, B. K.; Sohn, K.-S.; Pyo, M. *J. Electrochem. Soc.* **2012**, *159*, A1867. (c) Prabakar, S. J. R.; Hwang, Y.-H.; Bae, E. G.; Lee, D. K.; Pyo, M. *Carbon* **2013**, *52*, 128. (d) Lee, D. K.; Han, S. C.; Ahn, D.; Singh, S. P.; Sohn, K.-S.; Pyo, M. *ACS Appl. Mater. Interf.* **2013**, *4*, 6842. (e) Kim, H. S.; Kim, S.-O.; Kim, Y.-T.; Jung, J. K.; Na, B. K.; Lee, J. K. *Bull. Korean Chem. Soc.* **2012**, *33*, 65. (f) Lim, H.-H.; Cho, A.-R. Sivakumar, N.; Kim, W.-S.; Yoon, W.-S.; Lee, Y.-S. *Bull. Korean Chem. Soc.* **2011**, *32*, 1491.
3. (a) Zhang, W.-J. *J. Power Sources* **2011**, *196*, 13.
4. (a) Wang, G. X.; Ahn, J.; Lindsay, M. J.; Sun, L.; Bradhurst, D. H.; Dou, S. X.; Liu, H. K. *J. Power Sources* **2001**, *97-98*, 211. (b) Derrien, G.; Hassoun, J.; Panero, S.; Scrosati, B. *Adv. Mater.* **2007**, *19*, 2336. (c) Liang, S.; Zhu, X.; Lian, P.; Yang, W.; Wang, H. *J. Solid State Chem.* **2011**, *184*, 1400. (d) Wen, Z.; Cui, S.; Kim, H.; Mao, S.; Yu, K.; Lu, K.; Lu, G.; Pu, H.; Mao, O.; Chen, J. *J. Mater. Chem.* **2012**, *22*, 3300. (e) Wang, G.; Wang, B.; Wang, X.; Park, J.; Dou, S.; Ahn, H.; Kim, K. *J. Mater. Chem.* **2009**, *19*, 8378.

5. Van der Biest, O. O.; Vandeperre, L. J. *Ann. Rev. Mater. Sci*. **1999**, *29*, 327.
6. (a) Choi, H.; Kim, H.; Hwang, S.; Han, Y.; Jeon, M. *J. Mater. Chem*. **2011**, *21*, 7548. (b) Yin, X.; Xue, Z.; Liu, B. *J. Power Sources* **2011**, *196*, 2422.
7. (a) Wu, Z.-S.; Pei, S.; Ren, W.; Tang, D.; Gao, L.; Liu, B.; Li, F.; Liu, C.; Cheng, H.-M. *Adv. Mater*. **2009**, *21*, 1756. (b) Zhang, Y. A.; Lin, J. Y.; Wu, C. X.; Li, F. S.; Guo, T. L. *Solid-State Electron.* **2012**, *67*, 6. (c) Choi, W. B.; Jin, Y. W.; Kim, H. Y.; Lee, S. J.; Yun, M. J.; Kang, J. H.; Choi, Y. S.; Park, N. S.; Lee, N. S.; Kim, J. M. *Appl. Phys. Lett*. **2001**, *78*, 1547. (d) Zhao, H.; Song, H.; Li, Z.; Yuan, G.; Jin, Y. *Appl. Surf. Sci*. **2005**, *251*, 242.
8. (a) Shane, M. J.; Talbot, J. B.; Kinney, B. G.; Sluzky, E.; Hesse, K. R. *J. Colloid Interf. Sci.* **1994**, *165*, 334. (b) Russ, B. E.; Talbot, J. B. *J. Electrochem. Soc.* **1998**, *145*, 1253. (c) Khoo, E.; Lee, P. S.; Ma, J. *J. Eur. Ceram. Soc*. **2010**, *30*, 1139.
9. (a) Kanamura, K.; Goto, A.; Rho, Y. H.; Umegaki, T. *J. Power Sources* **2001**, *97-98*, 294. (b) Caballero, A.; Hernán, L.; Melero, M.; Morales, J.; Moreno, R.; Ferrari, B. *J. Power Sources* **2006**, *158*, 583. (c) Ui, K.; Funo, S.; Nagase, H.; Idemoto, Y.; Koura, N. *Electrochemistry* **2006**, *74*, 474.
10. (a) Koura, N.; Funo, S.; Tsuiki, H.; Idemoto, Y.; Ui, K.; Matsumoto, T. *J. Surf. Finish. Soc. Jpn.* **2002**, *53*, 683. (b) Ui, K.; Minami, T.; Ishikawa, K.; Idemoto, Y.; Koura, N. *J. Power Sources* **2005**, *146*, 698. (c) Ui, K.; Kawamura, S.; Kumagai, N. *Electrochim. Acta* **2012**, *76*, 383.
11. Yang, J.; Yan, X.; Chen, J.; Ma, H.; Sun, D.; Xue, Q. *RSC Adv.* **2012**, *2*, 9665.
12. (a) Mi, X.; Huang, G.; Xie, W.; Wang, W.; Liu, Y.; Gao, J. *Carbon* **2012**, *50*, 4856. (b) Hassan, H. M. A.; Abdelsayed, V.; Khder, A. E. R. S.; Abouzeid, K. M.; Terner, J.; El-Shall, M. S.; Al-Resayes, S. I.; El-Azhary, A. A. *J. Mater. Chem*. **2009**, *19*, 3832.
13. Li, X.; Wang, H.; Robinson, J. T.; Sanchez, H.; Diankov, G.; Dai, H. *J. Am. Chem. Soc.* **2009**, *131*, 15939.
14. (a) Teng, C.-C.; Ma, C.-C. M.; Lu, C.-H.; Yang, S.-Y.; Lee, S.-H.; Hsiao, M.-C.; Yen, M.-Y.; Chiou, K.-C.; Lee, T.-M. *Carbon* **2011**, *49*, 5107. (b) Wang, Y.; Shi, Z.; Yu, J.; Chen, L.; Zhu, J.; Hu, Z. *Carbon* **2012**, *50*, 5525.
15. Wang, S.; Jiang, S. P.; Wang, X. *Electrochim. Acta* **2011**, *56*, 3338.
16. Ye, J.; Zhang, H.; Chen, Y.; Cheng, Z.; Hu, L.; Ran, Q. *J. Power Sources* **2012**, *212*, 105.
17. Wolfenstine, J. *J. Power Sources* **1999**, *79*, 111.
18. Xu, Y.; Zhu, Y.; Liu, Y.; Wang, C. *Adv. Energ. Mater*. **2013**, *3*, 128.